Ukrainian Journal of Physical Optics
ISSUE 1
2027

# CUBIC-QUARTIC OPTICAL SOLITONS WITH COMPLEX GINZBURG-LANDAU EQUATION HAVING POWER-LAW OF SELF-PHASE MODULATION AND FRACTIONAL TEMPORAL EVOLUTION

**MOHAMED SHARAF [1], MOHAMED E. M. ALNGAR [2], REHAM M. A. SHOHIB [3], HOURIA TRIKI [4], SYED ASIF ALI SHAH [5] & ANJAN BISWAS [6,7,8,9]**

[1] Department of Industrial Engineering, College of Engineering, King Saud University, Riyadh 12372, Saudi Arabia
[2] Mathematics Education Program, Faculty of Education and Arts, Sohar University, Sohar 311, Oman
[3] Basic Science Department, Faculty of Economics and Business Administration, Innovation University, Sharqia, Egypt
[4] Radiation Physics Laboratory, Department of Physics, Faculty of Sciences, Badji Mokhtar University, P. O. Box 12, 23000 Annaba, Algeria
[5] Interdisciplinary Research Center for Intelligent Secure Systems (IRC-ISS), King Fahd University of Petroleum and Minerals (KFUPM), Dhahran, 31261, Saudi Arabia
[6] Department of Mathematics and Physics, Grambling State University, Grambling, LA 71245–2715, USA
[7] Department of Mathematics, Faculty of Science, Karadeniz Technical University, Trabzon–61080, Türkiye
[8] Department of Physics and Electronics, Khazar University, Baku, AZ–1096, Azerbaijan
[9] Applied Science Research Center, Applied Science Private University, Amman–11937, Jordan

**Received**: 17.10.2026

**Abstract.** This study investigates optical solitons governed by a conformable time-fractional complex Ginzburg-Landau equation with power-law self-phase modulation. The model incorporates third- and fourth-order dispersion, intermodal dispersion, self-steepening, and nonlinear dispersive perturbations. A conformable traveling-wave transformation reduces the governing equation to a fourth-order nonlinear ordinary differential equation, while consistency between its real and imaginary components yields explicit compatibility and integrability conditions. The extended auxiliary equation method is then employed to construct exact bright, dark, and singular solitons, together with periodic solutions expressed in terms of Jacobi and Weierstrass elliptic functions. The corresponding existence conditions are presented explicitly. Graphical representations illustrate how the conformable fractional order modifies the effective temporal scaling, phase structure, and propagation trajectories of representative bright and dark solitons. The derived solutions extend the analytical description of nonlinear waves in higher-order dispersive optical systems and may serve as benchmarks for future numerical and stability investigations.

**Keywords:** Optical solitons, fractional complex Ginzburg-Landau equation, power-law nonlinearity, cubic-quartic dispersion, extended auxiliary equation method, elliptic-function solutions

**UDC:** 530.182+535.3, 517.9
**DOI:** 10.3116/16091833/Ukr.J.Phys.Opt.2027.01089
This work is licensed under the Creative Commons Attribution International License (CC BY 4.0).

## 1. Introduction

Optical solitons constitute an important class of localized nonlinear waves that arise in dispersive optical media and transmission systems [1-3]. These self-sustaining wave packets can maintain their profiles over long propagation distances because the pulse-broadening effect of chromatic dispersion is balanced by nonlinear phase modulation. Since their discovery, optical solitons have attracted considerable theoretical and experimental interest owing to their potential applications in ultrahigh-speed communication, nonlinear photonics, optical switching, pulse shaping, and signal-processing technologies [4, 5].

Recent studies have substantially advanced the analytical description of soliton dynamics in complex and dispersive media. Proportional vector quiescent solitons in a coupled nonlinear Schrödinger system incorporating Kerr-type self-phase modulation, cross-phase modulation, and nonlinear dispersion were investigated in [6], where several exact wave families were derived, and the numerical stability of a representative bright-soliton branch was examined. Lie-symmetry analysis combined with a generalized auxiliary-equation method was applied in [7] to construct hyperbolic, exponential, and Jacobi elliptic solutions of a perturbed Schrödinger-Hirota equation. Lie-symmetry reductions were also employed to derive implicit quiescent-soliton solutions and their existence conditions for nonlinear Schrödinger and complex Ginzburg-Landau models describing optical metamaterials [8]. Earlier investigations produced bright, dark, singular, and twin-singular highly dispersive solitons under Kudryashov's sextic-power refractive-index law [9], as well as bright-dark Thirring combo solitons in birefringent fibers with cubic nonlinearity and spatiotemporal dispersion [10]. More recently, a modified sub-ODE method was used to obtain bright, dark, singular, periodic, and elliptic-function solutions for a stochastic (3+1)-dimensional coupled nonlinear Schrödinger model of fiber Bragg-grating media [11]. Nonlinear pulse propagation in modern optical systems is commonly modelled by evolution equations that incorporate the competing effects of dispersion, nonlinearity, dissipation, gain, and higher-order perturbations [12,13]. Among these models, the complex Ginzburg-Landau equation (CGLE) occupies a prominent position because it provides a general mathematical framework for describing nonlinear waves in optical fibers, mode locked lasers, dissipative media, plasma systems, and Bose-Einstein condensates. A broad range of analytical and numerical techniques has consequently been developed to investigate the exact solutions, numerical approximations, bifurcation structures, stability properties, and chaotic dynamics associated with different forms of the CGLE [14-21].

Fractional extensions of the CGLE provide additional flexibility for describing wave evolution when the temporal scaling departs from that of the conventional integer-order model. In the conformable formulation adopted here, the fractional-order parameter modifies the effective time variable and, consequently, the propagation trajectory and phase evolution of the optical field. The classical model is recovered when the fractional order approaches unity. In particular, fractional parameters can modify the spatial and temporal scaling of the solutions and thereby alter their localization, phase, and propagation characteristics. The present work considers a conformable fractional CGLE with power-law nonlinearity and incorporates higher-order dispersion, self-steepening, and nonlinear dispersive perturbations. Related fractional CGLEs with Kerr and non-Kerr nonlinearities have been examined in [22-24], demonstrating that fractional-order models support a wide variety of localized structures. Within the conformable framework adopted here, the fractional order serves as a tunable parameter governing the effective evolution of the optical field and recovering the corresponding classical model in the integer-order limit.

To construct exact analytical solutions of the governing equation, the extended auxiliary expansion method is employed. This technique provides a systematic procedure for reducing the nonlinear evolution equation to an auxiliary ordinary differential equation and matching the resulting coefficients. The method and its related formulations have proved effective for variable-coefficient Korteweg-de Vries (KdV) equations and several nonlinear Schrödinger-

type models [25-27]. In the present analysis, it generates bright, dark, singular, Jacobi elliptic, and Weierstrass elliptic wave solutions together with the parameter constraints required for their existence.

Although auxiliary expansion and algebraic techniques have been widely utilized for standard integer-order and lower-order fractional Schrödinger-type models, the existing literature lacks a comprehensive analytical treatment of the conformable time-fractional CGLE incorporating both cubic-quartic dispersion and power-law self-phase modulation. The primary novelty of this work is mapping this highly generalized, multi-parameter evolution equation to exact bright, dark, singular, and elliptic-function solutions via a rigorous non-integer transformation scheme. By establishing the explicit parameter existence criteria and illustrating the role of the fractional temporal order on pulse trajectories, this study bridges the gap between generalized higher-order nonlinear optics and fractional analytical modeling.

The remainder of this paper is organized as follows. Section 2 introduces the governing mathematical model. Section 3 presents the preliminary analysis and the main steps of the extended auxiliary expansion method. Section 4 derives the exact soliton and elliptic-function solutions. Section 5 discusses their physical characteristics and the effects of the relevant parameters. Finally, Section 6 summarizes the study's principal conclusions.

## 2. Mathematical model

The present study considers a higher-order nonlinear evolution model for optical-wave propagation in dispersive media with power-law self-phase modulation. The governing equation is a conformable time-fractional complex Ginzburg-Landau equation incorporating third- and fourth-order dispersion, intermodal dispersion, self-steepening, and nonlinear dispersive perturbations. The conformable fractional order introduces a nonlinear temporal rescaling, while the corresponding integer-order model is recovered when $\eta = 1$. The governing equation is expressed as follows:

$$i\frac{\partial^{\eta} q}{\partial t^{\eta}} + iaq_{xxx} + bq_{xxxx} + c\,|q|^{2n} q = \sigma\frac{|q_x|^2}{q^*} + \frac{1}{|q|^2 q^*}\left[\alpha\,|q|^2 (|q|^2)_{xx} - \beta\left[\left((|q|^2)_x\right)\right]^2\right] + \gamma q + i\left[\delta q_x + \lambda\left(|q|^2 q\right)_x + \mu\left(|q|^2\right)_x q + \theta\,|q|^2 q_x\right]. \quad (1)$$

Here, $q = q(x,t)$ denotes the complex optical-field envelope, while $x$ and $t$ represent the spatial and temporal variables, respectively.

In Eq. (1), the first term, where $= \sqrt{-1}$, governs the temporal evolution of the optical field. The coefficients $a$ and $b$ characterize the third-order and fourth-order dispersion effects, respectively. The coefficient $c$ characterizes the power-law self-phase modulation, where $n > 0$ is the nonlinearity exponent. The standard Kerr response is recovered as the special case $n = 1$. Moreover, $\gamma$ denotes the detuning parameter, while $\delta$ accounts for intermodal dispersion. The parameter $\lambda$ describes the self-steepening effect, whereas $\mu$ and $\theta$ represent higher-order nonlinear dispersive contributions associated with derivative-nonlinear terms (specifically governing combined phase-steepening and intensity-dependent dispersion interactions). Furthermore, the coefficients $\sigma$, $\alpha$, and $\beta$ quantify additional nonlinear interaction and dispersion mechanisms: $\sigma$ measures the nonlinear dispersion, while $\alpha$ and $\beta$ quantify higher-order perturbative nonlinear interactions associated with the second-order spatial derivatives of the optical intensity. Together, these mechanisms

influence the propagation dynamics, phase evolution, and structural stability of the resulting optical solitons.

To clarify the physical classification of Eq. (1) within the complex Ginzburg-Landau framework, we note that the parameter $\gamma$ functions as the linear gain-loss or detuning coefficient, while the higher-order derivative terms ($\mu,\theta,\sigma,\alpha,\beta$) introduce nonlinear dispersion, phase-steepening, and non-conservative perturbation processes. These terms account for the necessary energy exchange between the optical field and a dissipative or active medium. Furthermore, dimensional consistency across the governing equation is preserved by scaling the spatial derivatives, temporal derivative ($t^{\eta}$), and power-law nonlinearity ($c|q|^{2n}q$) such that every term shares a consistent equivalent dimension with respect to the field amplitude $q$ and propagation coordinates.

For $t>0$ and $0<\eta\le 1$, the conformable fractional derivative introduced by Khalil et al. [28] is defined as $T_{\eta}(f)(t)=\lim_{\varepsilon\to 0}\dfrac{f\left(t+\varepsilon t^{1-\eta}\right)-f(t)}{\varepsilon}$. For every classically differentiable function $f$, this definition satisfies $T_{\eta}(f)(t)=t^{1-\eta}\dfrac{df}{dt}$. Accordingly, $\eta$ modifies the temporal scaling of the optical field, while the classical first-order derivative is recovered when $\eta=1$.

## 3. Preliminary analysis

To investigate the propagation behavior of the optical pulses, we employ the traveling-wave transformation within the framework of conformable fractional calculus

$$q(x,t)=u(\zeta)e^{ir(x,t)},\ \zeta=x-\frac{vt^{\eta}}{\eta},\ r(x,t)=-\kappa x+\frac{\omega t^{\eta}}{\eta}+\zeta_0, \tag{2}$$

where $0<\eta\le 1$. Here, $u(\zeta)$ denotes the real-valued wave profile, while $r(x,t)$ is the corresponding phase function. The traveling-wave variable $\zeta$ combines the spatial coordinate with the fractional temporal evolution, where $v$ is the wave velocity. The fractional parameter $\eta$ controls the conformable temporal scaling through $t^{\eta}/\eta$, thereby modifying the effective propagation trajectory and phase evolution. The transformation is considered for $t>0$ and reduces to the classical traveling-wave variable when $\eta=1$. In addition, $\kappa,\omega$, and $\zeta_0$ denote the wave number, angular frequency, and an arbitrary phase constant, respectively.

Substituting Eq. (2) into Eq. (1) and separating the resulting equation into its real and imaginary parts yields:

$$\begin{aligned}&\Re: bu''''(\zeta)+\left[3\kappa(a-2b\kappa)-2\alpha\right]u''(\zeta)-\left(-b\kappa^4+a\kappa^3+\sigma\kappa^2+\delta\kappa+\gamma+\omega\right)u(\zeta)\\&-\kappa(\theta+\lambda)u^3(\zeta)+cu^{2n+1}(\zeta)+(4\beta-\sigma-2\alpha)\frac{u'^2(\zeta)}{u(\zeta)}=0,\end{aligned} \tag{3}$$

and

$$\Im:(a-4b\kappa)u'''(\zeta)+(4b\kappa^3-3a\kappa^2-v-\delta)u'(\zeta)-(\theta+2\mu+3\lambda)u^2(\zeta)u'(\zeta)=0. \tag{4}$$

To obtain a nontrivial traveling-wave reduction that is compatible with the adopted real-amplitude ansatz, we impose the following sufficient parameter conditions:

$$a = 4b\kappa,\ \theta + 2\mu + 3\lambda = 0,\\ v = -8b\kappa^3 - \delta. \tag{5}$$

In Eq. (3), the non-polynomial derivative term $u'^2(\zeta)/u(\zeta)$ introduces a mathematical singularity whenever the field amplitude $u(\zeta) \to 0$. In physical optical transmission systems, such singularities can lead to unphysical blow-up behavior or infinite local intensities unless appropriately balanced or eliminated.

Thus, we impose the simplifying condition:

$$4\beta - \sigma - 2\alpha = 0. \tag{6}$$

Substituting Eqs. (5) and (6) into Eq. (3) reduces the governing equation to the fourth-order ordinary differential equation:

$$bu''''(\zeta) + 2(3b\kappa^2 - \alpha)u''(\zeta) - [3b\kappa^4 + \sigma\kappa^2 + \delta\kappa + \gamma + \omega]u(\zeta)\\ -\kappa(\theta + \lambda)u^3(\zeta) + cu^{2n+1}(\zeta) = 0. \tag{7}$$

To facilitate the subsequent analysis, we introduce the transformation

$$u(\zeta) = V^{\frac{2}{n}}(\zeta). \tag{8}$$

For the real-valued representation $V(\zeta) > 0$ is required so that $V^{2/n}$ remains real.

It is important to emphasize that the inclusion of the general power-law exponent $n$ in Eq. (7) introduces non-polynomial derivative terms. The transformation (8) is thus crucial for linearizing and decoupling these terms into the generalized auxiliary polynomial form.

By substituting (8) into Eq. (7), we obtain a new equation:

$$2bn^3V^3(\zeta)V''''^{(\zeta)} - 8bn^2(n-2)V^2(\zeta)V'(\zeta)V'''(\zeta) - 6bn^2(n-2)V^2(\zeta)V''^2(\zeta)\\ -4b(3n-2)(n-2)(n-1)V'^4(\zeta) - \kappa(\theta+\lambda)n^4V(\zeta)^{\frac{4+4n}{n}}\\ +2n[12b(n-1)(n-2)V'^2(\xi) + 2n^2(3b\kappa^2 - \alpha)V^2(\zeta)]V(\xi)V''(\xi)\\ -4n^2(3b\kappa^2 - \alpha)(n-2)V^2(\zeta)V'^2(\zeta)\\ -n^4V^4(\zeta)(3b\kappa^4 + \sigma\kappa^2 + \delta\kappa + \gamma + \omega - cV^4(\zeta)) = 0 \tag{9}$$

To ensure integrability, it is imperative to choose:

$$\theta = -\lambda. \tag{10}$$

Without eliminating this cubic term, the ordinary differential equation cannot be easily reduced or mapped to standard auxiliary forms, meaning balanced, stable solitons cannot be analytically constructed for this specific parameter configuration. Thus, Eq. (9) converts into:

$$2bn^3V^3(\zeta)V''''(\zeta) - 8bn^2(n-2)V^2(\zeta)V'(\zeta)V'''(\zeta) - 6bn^2(n-2)V^2(\zeta)V''^2(\zeta)\\ +2n[12(n-1)(n-2)bV'^2(\zeta) + n^2\Pi V^2(\zeta)]V(\zeta)V''(\zeta)\\ -4(3n-2)(n-1)(n-2)bV'^4(\zeta) - 2n^2(n-2)\Pi V^2(\zeta)V'^2(\zeta)\\ -n^4V^4(\zeta)[\Theta - cV^4(\zeta)] = 0, \tag{11}$$

where

$$\Pi = 2(3b\kappa^2 - \alpha), \quad \Theta = 3b\kappa^4 + \sigma\kappa^2 + \delta\kappa + \gamma + \omega. \tag{12}$$

To construct exact solutions of Eq. (11), the extended auxiliary equation method assumes a finite-series representation of the form [25-27]:

$$V(\zeta)=\sum_{i=0}^{N}H_i\mathcal{F}^i(\zeta), \tag{13}$$

where the auxiliary function $\mathcal{F}(\zeta)$ satisfies the first-order nonlinear differential equation

$$\left[\mathcal{F}'(\zeta)\right]^2=\sum_{j=0}^{4}r_j\mathcal{F}^j(\zeta). \tag{14}$$

Here, $H_i$ and $r_j$ are constants satisfying $H_N\neq 0$ and $r_4\neq 0$, while $N\in\mathbb{Z}^+$. Depending on the choices of the parameters $r_j$, Eq. (14) admits several families of hyperbolic, Jacobi elliptic, and Weierstrass elliptic function solutions, as summarized below.

**Set 1**: For $r_0=r_1=r_3=0$, Eq. (14) admits the following solutions:

**(I) Bright-soliton solution**

$$\mathcal{F}(\zeta)=\pm\sqrt{-\frac{r_2}{r_4}}\operatorname{sech}\left(\sqrt{r_2}\zeta\right).\ r_2>0,\ r_4<0. \tag{15}$$

**(II) Singular-soliton solution**

$$\mathcal{F}(\zeta)=\pm\sqrt{\frac{r_2}{r_4}}\operatorname{csch}\left(\sqrt{r_2}\zeta\right).\ r_2>0,\ r_4>0. \tag{16}$$

**Set 2:** For $r_1=r_3=0, r_0=\frac{r_2^2}{4r_4}$, Eq. (14) yields the following solutions:

**(I) Dark-soliton solution**

$$\mathcal{F}(\zeta)=\pm\sqrt{-\frac{r_2}{2r_4}}\tanh\left(\sqrt{-\frac{r_2}{2}}\zeta\right).\ r_2\langle 0,\ r_4\rangle 0. \tag{17}$$

**(II) Singular-soliton solution**

$$\mathcal{F}(\zeta)=\pm\sqrt{-\frac{r_2}{2r_4}}\coth\left(\sqrt{-\frac{r_2}{2}}\zeta\right).\ r_2\langle 0,\ r_4\rangle 0. \tag{18}$$

**Set 3:** For $r_1=r_3=0, r_0=\frac{r_2^2M}{r_4}$, Eq. (14) admits Jacobi elliptic function solutions:

**(I)** For $M=-\frac{m^2(1-m^2)}{(2m^2-1)^2}$ :

$$\mathcal{F}(\zeta)=\pm\sqrt{-\frac{m^2r_2}{(2m^2-1)r_4}}\operatorname{cn}\left(\sqrt{-\frac{r_2}{2m^2-1}}\zeta,m\right),\ (2m^2-1)r_2\langle 0,\ r_4\rangle 0. \tag{19}$$

**(II)** For $M=\frac{1-m^2}{(2-m^2)^2}$ :

$$\mathcal{F}(\zeta)=\pm\sqrt{-\frac{r_2}{(2-m^2)r_4}}\operatorname{dn}\left(\sqrt{\frac{r_2}{2-m^2}}\zeta,m\right),\ r_2>0,\ r_4<0. \tag{20}$$

**(III)** For $M=\frac{m^2}{(1+m^2)^2}$ :

$$\mathcal{F}(\zeta)=\pm\sqrt{-\frac{m^2r_2}{(1+m^2)r_4}}\operatorname{sn}\left(\sqrt{\frac{r_2}{1+m^2}}\zeta,m\right),\ r_2>0,\ r_4<0. \tag{21}$$

Here, $m$ denotes the elliptic modulus, with $0\le m\le 1$.

**Set 4:** For $r_1 = r_3 = 0$, Eq. (14) also admits solutions expressed in terms of the Weierstrass elliptic function:

**(I)** If $g_2 = r_0 r_4 + \frac{r_2^2}{12}, g_3 = \frac{r_2\left(36 r_0 r_4 - r_2^2\right)}{216}$, then

$$\mathcal{F}(\zeta) = \frac{3\wp'(\zeta; g_2, g_3)}{\sqrt{r_4}\left[6\wp(\zeta; g_2, g_3) + r_2\right]}, \; r_4 > 0. \tag{22}$$

**(II)** If $g_2 = \frac{4}{3} r_2^2 - 3 r_0 r_4, \; g_3 = \frac{4}{27}\left(9 r_0 r_2 r_4 - 2 r_2^3\right)$, then

$$\mathcal{F}(\zeta) = \sqrt{\frac{3\wp(\zeta; g_2, g_3) - r_2}{3 r_4}}. \tag{23}$$

Here, $\wp(\zeta; g_2, g_3)$ denotes the Weierstrass elliptic function, and

$$\wp'(\zeta; g_2, g_3) = \frac{d}{d\zeta}\wp(\zeta; g_2, g_3). \tag{24}$$

The Weierstrass elliptic function satisfies

$$\left[\wp'(\zeta; g_2, g_3)\right]^2 = 4\wp^3(\zeta; g_2, g_3) - g_2\wp(\zeta; g_2, g_3) - g_3, \tag{25}$$

where $g_2$ and $g_3$ are the corresponding Weierstrass invariants.

## 4. Application of the extended auxiliary equation method

To determine the truncation order $N$, we apply the homogeneous-balance principle to the highest-order derivative contribution $V^3 V''''$ and the highest-degree nonlinear contribution $V^8$ in Eq. (11). Thus:

$$N = 1. \tag{26}$$

Consequently, the general expansion introduced in Eq. (13) reduces to

$$V(\zeta) = H_0 + H_1 \mathcal{F}(\zeta), \; H_1 \neq 0, \tag{27}$$

where $H_0$ and $H_1$ are constants to be determined.

Substituting Eqs. (27) and (14) into the reduced governing equation (11), collecting terms with identical powers of $\mathcal{F}(\zeta)$, and setting the coefficient of each independent power equal to zero leads to the following nonlinear algebraic system:

$$\begin{aligned}
&(n+1)(n+2)\left(n+\frac{2}{3}\right) b r_4^2 + \frac{1}{12} n^4 H_1^4 c = 0, \\
&n H_0 b (n+2)(n+1) r_4^2 + \frac{1}{4} H_1 (n+1)(n+2)\left(n+\frac{4}{3}\right) r_3 b r_4 + \frac{1}{6} n^4 H_0 H_1^4 c = 0, \\
&\left[\left(\frac{35}{8} c H_0^4 - \frac{1}{16}\Theta\right) n^4 + \left(\left(\frac{5}{8} r_3 r_1 + \frac{5}{2} r_4 r_0\right) b + \frac{1}{4}\Pi r_2\right) n^2 + b\left(r_2^2 + 2 r_3 r_1 + 2 r_4 r_0\right)\right] H_1^3 \\
&+ \frac{5}{16}\left[\left((6 r_1 r_4 + r_2 r_3) b + \Pi r_3\right) n^2 + \left(\left(12 r_1 r_4 + 4 r_2 r_3\right) b + \frac{8}{5}\Pi r_3\right) n + 24 b\left(r_1 r_4 + r_2 r_3\right)\right] n H_0 H_1^2 \\
&+ \frac{5}{2}\left[\left(\left(r_2 r_4 + \frac{3}{16} r_3^2\right) b + \frac{1}{4}\Pi r_4\right) n + \left(\left(\frac{15}{8} r_3^2 + 4 r_2 r_4\right) b + \frac{1}{10}\Pi r_4\right)\right] n^2 H_0^2 H_1 \\
&+ \frac{15}{4} b n^3 H_0^3 r_3 r_4 = 0,
\end{aligned} \tag{28}$$

$$
\begin{aligned}
&(n-2)\left[\left(r_0r_2+\frac{3}{16}r_1^2\right)b+\frac{1}{4}\Pi r_0\right]n^2H_1^3\\
&+(n-2)\left[b\left(-2r_0r_2-r_1^2\right)n+b\left(2r_0r_2+r_1^2\right)\right]H_1^3\\
&-\frac{11}{8}n\begin{Bmatrix}\left[\left(r_2r_1+\frac{6}{11}r_3r_0\right)b-\frac{1}{11}\Pi r_1\right]n^2\\+\left[\left(-\frac{52}{11}r_2r_1-\frac{12}{11}r_3r_0\right)b+\frac{8}{11}\Pi r_1\right]n+\frac{72}{11}b\left(r_3r_0+r_2r_1\right)\end{Bmatrix}H_0H_1^2\\
&+n^2\begin{Bmatrix}\left(-\frac{7}{2}cH_0^4+\frac{3}{4}\Theta\right)n^2+\left[\left(r_2^2+\frac{3}{4}r_3r_1-3r_4r_0\right)b-\frac{1}{2}\Pi r_2\right]n\\+\left(-\frac{33}{4}r_3r_1-12r_4r_0-\frac{7}{2}r_2^2\right)b-\frac{1}{2}\Pi r_2\end{Bmatrix}H_0^2H_1\\
&-\frac{15}{8}\left[\left(2r_1r_4+r_2r_3\right)b+\frac{1}{5}\Pi r_3\right]n^3H_0^3=0,
\end{aligned}
$$

$$
\begin{aligned}
&-\frac{1}{2}(n-4)\begin{bmatrix}\left(\left(6r_3r_0+r_2r_1\right)b+\Pi r_1\right)n^2\\-4b\left(r_3r_0+r_2r_1\right)n+8b\left(r_3r_0+r_2r_1\right)\end{bmatrix}H_1^3+nH_0H_1^2\\
&\begin{Bmatrix}\left(-2\Theta+28cH_0^4\right)n^3+\left[\left(r_2^2+\frac{9}{2}r_3r_1+12r_4r_0\right)b+\Pi r_2\right]n^2\\+\left[\left(-8r_2^2+24r_4r_0-6r_3r_1\right)b+4\Pi r_2\right]n\\+24b\left(r_2^2+2r_3r_1+2r_4r_0\right)\end{Bmatrix}\\
&-\frac{5}{2}\begin{Bmatrix}\left[\left(r_2r_3-6r_1r_4\right)b-\frac{7}{5}\Pi r_3\right]n\\+\left(-24r_1r_4-20r_2r_3\right)b-\frac{4}{5}\Pi r_3\end{Bmatrix}n^2H_0^2H_1+20\left[\left(\frac{3}{8}r_3^2+r_2r_4\right)b+\frac{1}{10}\Pi r_4\right]n^3H_0^3=0,
\end{aligned}
\qquad \text{(28, cont.)}
$$

$$
\begin{aligned}
&\frac{7}{18}n^4H_0^2H_1^4c+\frac{1}{9}(n+2)\begin{Bmatrix}\left[\left(r_2r_4+\frac{3}{16}r_3^2\right)b+\frac{1}{4}\Pi r_4\right]n^2\\+b\left(2r_2r_4+r_3^2\right)n+b\left(2r_2r_4+r_3^2\right)\end{Bmatrix}H_1^2\\
&+\frac{2}{3}H_0r_4(n+2)\left(n+\frac{7}{4}\right)nr_3bH_1+bn^2H_0^2r_4^2(n+2)=0,
\end{aligned}
$$

$$
\begin{aligned}
&\left(4H_0^7c-2H_0^3\Theta\right)n^4+\begin{Bmatrix}\left[\left(r_2^2+\frac{9}{2}r_3r_1+12r_4r_0\right)b+\Pi r_2\right]H_0^3\\-\frac{11}{2}\left[\left(r_2r_1+\frac{6}{11}r_3r_0\right)b-\frac{1}{11}\Pi r_1\right]H_1H_0^2\\+4\left[\left(r_0r_2+\frac{9}{8}r_1^2\right)b-\frac{1}{2}\Pi r_0\right]H_1^2H_0-6bH_1^3r_0r_1\end{Bmatrix}n^3\\
&+14\begin{Bmatrix}\left[\left(\frac{12}{7}r_3r_0+r_2r_1\right)b+\frac{1}{7}\Pi r_1\right]H_0^2+16bH_1^3r_0r_1\\-\frac{10}{7}H_0H_1\left[\left(\frac{3}{4}r_1^2+r_0r_2\right)b-\frac{1}{5}\Pi r_0\right]+\frac{13}{7}br_0r_1H_1^2\end{Bmatrix}H_1n^2\\
&+24\left[\left(r_0r_2+\frac{1}{2}r_1^2\right)H_0-\frac{3}{2}r_0r_1H_1\right]H_1^2bn=0,
\end{aligned}
$$

$$
\begin{aligned}
&\frac{1}{2}\left(-2H_0^4\Theta+2H_0^8c\right)n^4\\
&+H_1\left\{\begin{matrix}-12br_0^2H_1^3+12H_0br_0r_1H_1^2-8\left[\left(r_0r_2+\frac{3}{16}r_1^2\right)b+\frac{1}{4}\Pi r_0\right]H_0^2H_1\\+\left[\left(6r_3r_0+r_2r_1\right)b+\Pi r_1\right]H_0^3\end{matrix}\right\}n^3\\
&+16H_1^2\left\{\frac{11}{4}br_0^2H_1^2-\frac{9}{4}H_0br_0r_1H_1+\left[\left(r_0r_2+\frac{3}{16}r_1^2\right)b+\frac{1}{4}\Pi r_0\right]H_0^2\right\}n^2\\
&+24bH_1^3r_0\left(r_1H_0-2H_1r_0\right)n+16bH_1^4r_0^2=0,\\
&\frac{7}{6}n^4H_0^3H_1^4c+\frac{1}{8}(n+4)\left\{\begin{matrix}\left[\left(\frac{1}{6}r_2r_3+r_1r_4\right)b+\frac{1}{6}\Pi r_3\right]n^2\\+\frac{2}{3}b\left(r_1r_4+r_2r_3\right)n+\frac{4}{3}b\left(r_1r_4+r_2r_3\right)\end{matrix}\right\}H_1^3\\
&+\frac{2}{3}H_0n\left\{\begin{matrix}\left[\left(r_2r_4+\frac{3}{16}r_3^2\right)b+\frac{1}{4}\Pi r_4\right]n^2\\+\left[\left(\frac{13}{4}r_2r_4+\frac{21}{16}r_3^2\right)b+\frac{1}{4}\Pi r_4\right]n+\frac{9}{2}\left(r_2r_4+\frac{1}{2}r_3^2\right)b\end{matrix}\right\}H_1^2\\
&+\frac{2}{2}br_4n^2H_0^2r_3(n+3)H_1+bn^3H_0^3r_4^2=0.
\end{aligned}
\tag{28, end}
$$

The resulting system determines the admissible values of $H_0, H_1$, and the auxiliary-equation parameters $r_0, r_1, r_2, r_3$, and $r_4$, along with the associated constraints on the physical parameters.

**Family 1.** Setting $r_0 = r_1 = r_3 = 0$ in Eq. (28) and solving the resulting algebraic system symbolically using Maple yields

$$
H_0 = 0,\ H_1 = \left[-\frac{\left(12n^3+44n^2+48n+16\right)br_4^2}{cn^4}\right]^{\frac{1}{4}},\ r_2 = -\frac{n^2\Pi}{4b\left(n^2+2n+2\right)},
\tag{29}
$$

together with

$$
\Theta = -\frac{\Pi^2(n+1)^2}{b\left(n^2+2n+2\right)^2},
\tag{30}
$$

subject to the condition $bc<0$. Substituting Eq. (29), together with Eqs. (15) and (16), into Eq. (27) gives the following exact soliton solutions of Eq. (1):

**(I) Bright-soliton solution**

$$
q(x,t) = \left[\begin{matrix}\left(-\frac{3n^3+11n^2+12n+4}{bc}\right)^{\frac{1}{4}}\sqrt{\frac{\Pi}{2\left(n^2+2n+2\right)}}\\ \times sech\left(\frac{n}{2}\sqrt{-\frac{\Pi}{b\left(n^2+2n+2\right)}}\left(x-\frac{vt^\eta}{\eta}\right)\right)\end{matrix}\right]^{\frac{2}{n}}\exp\left[i\left(-\kappa x+\frac{\omega t^\eta}{\eta}+\zeta_0\right)\right].
\tag{31}
$$

**(II) Singular-soliton solution**

$$
q(x,t) = \left[\begin{matrix}\left(-\frac{3n^3+11n^2+12n+4}{bc}\right)^{\frac{1}{4}}\sqrt{\frac{\Pi}{2\left(n^2+2n+2\right)}}\\ \times csch\left(\frac{n}{2}\sqrt{-\frac{\Pi}{b\left(n^2+2n+2\right)}}\left(x-\frac{vt^\eta}{\eta}\right)\right)\end{matrix}\right]^{\frac{2}{n}}\exp\left[i\left(-\kappa x+\frac{\omega t^\eta}{\eta}+\zeta_0\right)\right].
\tag{32}
$$

These solutions are valid under the parameter restrictions $\Pi > 0,\ b\langle 0,\ c\rangle 0$.

**Family 2.** For $r_1 = r_3 = 0,\ r_0 = r_2^2/4r_4$, the algebraic system (28) yields:

$$H_0 = 0,\ H_1 = \left(-\frac{24br_4^2}{c}\right)^{\frac{1}{4}},\ r_2 = -\frac{\Pi}{10b}, \tag{33}$$

and

$$\Theta = -\frac{3\Pi^2}{50b},\ n = 2, \tag{34}$$

with $bc < 0$. Upon substituting Eq. (33) and Eqs. (17,18) into Eq. (27), two additional exact solutions are obtained:

**(I) Dark-soliton solution**

$$q(x,t) = \left(-\frac{3}{2bc}\right)^{\frac{1}{4}}\sqrt{\frac{\Pi}{5}}\tanh\left[\frac{1}{2}\sqrt{\frac{\Pi}{5b}}\left(x - \frac{vt^{\eta}}{\eta}\right)\right]\exp\left[i\left(-\kappa x + \frac{\omega t^{\eta}}{\eta} + \zeta_0\right)\right]. \tag{35}$$

**(II) Singular-soliton solution**

$$q(x,t) = \left(-\frac{3}{2bc}\right)^{\frac{1}{4}}\sqrt{\frac{\Pi}{5}}\coth\left[\frac{1}{2}\sqrt{\frac{\Pi}{5b}}\left(x - \frac{vt^{\eta}}{\eta}\right)\right]\exp\left[i\left(-\kappa x + \frac{\omega t^{\eta}}{\eta} + \zeta_0\right)\right]. \tag{36}$$

The above solutions exist under the restrictions $\Pi > 0,\ b > 0,\ c < 0$.

**Family 3.** Consider $r_1 = r_3 = 0,\ r_0 = r_2^2 M/r_4$. Substitution into Eq. (28) yields the same parameter values as in Eq. (33), while the corresponding value of $\Theta$ becomes

$$\Theta = -\frac{3(4M-3)\Pi^2}{100b},\ n = 2. \tag{37}$$

Using Eq. (33) together with Eqs. (19-21) in Eq. (27) generates three classes of Jacobi elliptic-function solutions.

**(I)** For $M = -\dfrac{m^2(1-m^2)}{(2m^2-1)^2}$, one obtains

$$\begin{aligned} q(x,t) &= m\left(-\frac{3}{2bc}\right)^{\frac{1}{4}}\sqrt{\frac{2\Pi}{5(2m^2-1)}}\,\mathrm{cn}\left(\sqrt{-\frac{\Pi}{10b(2m^2-1)}}\left(x - \frac{vt^{\eta}}{\eta}\right), m\right) \\ &\exp\left[i\left(-\kappa x + \frac{\omega t^{\eta}}{\eta} + \zeta_0\right)\right], \end{aligned} \tag{38}$$

provided that

$$\Theta = -\frac{3\Pi^2}{100b}\left[\frac{4m^2(1-m^2)}{(2m^2-1)^2} + 3\right],\ \Pi(2m^2-1) > 0,\ b\langle 0,\ c\rangle 0. \tag{39}$$

**(II)** For $M = (1-m^2)/(2-m^2)^2$, the corresponding solution is

$$\begin{aligned} q(x,t) &= \left(-\frac{3}{2bc}\right)^{\frac{1}{4}}\sqrt{\frac{2\Pi}{5(2-m^2)}}\,\mathrm{dn}\left(\sqrt{-\frac{\Pi}{10b(2-m^2)}}\left(x - \frac{vt^{\eta}}{\eta}\right), m\right) \\ &\exp\left[i\left(-\kappa x + \frac{\omega t^{\eta}}{\eta} + \zeta_0\right)\right], \end{aligned} \tag{40}$$

where

$$\Theta=\frac{3\Pi^2}{100b}\left[\frac{4\left(1-m^2\right)}{\left(2-m^2\right)^2}-3\right],\ \Pi>0,\ b\langle 0,\ c\rangle 0. \tag{41}$$

**(III)** For $M=\dfrac{m^2}{\left(1+m^2\right)^2}$, we obtain

$$\begin{aligned} q(x,t)=m\left(-\frac{3}{2bc}\right)^{\frac{1}{4}}\sqrt{\frac{2\Pi}{5\left(m^2+1\right)}}\,\mathrm{sn}\left(\sqrt{\frac{\Pi}{10b\left(m^2+1\right)}}\left(x-\frac{vt^{\eta}}{\eta}\right),m\right) \\ \times\exp\left[i\left(-\kappa x+\frac{\omega t^{\eta}}{\eta}+\zeta_0\right)\right], \end{aligned} \tag{42}$$

subject to

$$\Theta=\frac{3\Pi^2}{100b}\left[\frac{4m^2}{\left(1+m^2\right)^2}-3\right],\ \Pi>0,\ b>0,\ c<0. \tag{43}$$

**Family 4.** Finally, imposing $r_1=r_3=0$ in Eq. (28) and solving the corresponding algebraic system using Maple gives

$$\begin{aligned} &H_0=0,\\ &H_1=\left[-\frac{\left(12n^3+44n^2+48n+16\right)br_4^2}{cn^4}\right]^{\frac{1}{4}},\\ &r_0=0,\\ &r_2=-\frac{n^2\Pi}{4b\left(n^2+2n+2\right)}, \end{aligned} \tag{44}$$

together with

$$\Theta=-\frac{\Pi^2(n+1)^2}{b\left(n^2+2n+2\right)^2}. \tag{45}$$

Substitution of Eq. (44) and Eqs. (22, 23) into Eq. (27) yields the following Weierstrass elliptic-function solutions of Eq. (1).

**(I)** If

$$\begin{aligned} g_2&=\frac{1}{3}\left[\frac{n^2\Pi}{8b\left(n^2+2n+2\right)}\right]^2,\\ g_3&=\left[\frac{n^2\Pi}{24b\left(n^2+2n+2\right)}\right]^3, \end{aligned} \tag{46}$$

then

$$q(x,t)=\left[\times\frac{\left(-\dfrac{4\left(3n^3+11n^2+12n+4\right)b}{n^4c}\right)^{\frac{1}{4}}\wp'\left(\left(x-\dfrac{vt^{\eta}}{\eta}\right),g_2,g_3\right)}{2\wp\left(\left(x-\dfrac{vt^{\eta}}{\eta}\right),g_2,g_3\right)-\dfrac{n^2\Pi}{12b\left(n^2+2n+2\right)}}\right]^{\frac{2}{n}}\exp\left[i\left(-\kappa x+\frac{\omega t^{\eta}}{\eta}+\zeta_0\right)\right]. \tag{47}$$

**(II)** If

$$g_2 = \frac{1}{3}\left[\frac{n^2\Pi}{2b\left(n^2+2n+2\right)}\right]^2, \qquad g_3 = \left[\frac{n^2\Pi}{6b\left(n^2+2n+2\right)}\right]^3, \tag{48}$$

then

$$q(x,t) = \left[\left(-\frac{4\left(3n^3+11n^2+12n+4\right)b}{n^4c}\right)^{\frac{1}{4}}\sqrt{\wp\left(\left(x-\frac{vt^\eta}{\eta}\right),g_2,g_3\right)+\frac{n^2\Pi}{12b\left(n^2+2n+2\right)}}\right]^{\frac{2}{n}} \times \exp\left[i\left(-\kappa x+\frac{\omega t^\eta}{\eta}+\zeta_0\right)\right]. \tag{49}$$

Overall, the extended auxiliary equation method yields a diverse set of exact solutions, including bright, dark, and singular solitons, as well as Jacobi and Weierstrass elliptic-function solutions. These results show the method's effectiveness in describing various nonlinear wave structures under appropriate parameter constraints.

To ensure the correctness and consistency of the exact solutions obtained, we independently verified them analytically and symbolically. For each principal family, the respective wave profile $u(\zeta)$ (or $V(\zeta)$) was substituted explicitly back into the reduced fourth-order nonlinear ordinary differential equation given by Eq. (11), and, applying the corresponding parameter constraints, all terms of Eq. (11) were confirmed to vanish identically. Furthermore, we cross-verified the complete algebraic systems and solution branches symbolically in Maple, ensuring that every constraint relation satisfies the underlying polynomial balance equations.

## 5. Physical interpretation

This section examines the physical characteristics of representative optical-soliton solutions obtained from the fractional complex Ginzburg-Landau equation. Particular attention is given to how the fractional order η affects the localization, phase structure, and propagation trajectory of the optical field. Three-dimensional surfaces, two-dimensional profiles, and contour plots of the absolute, real, and imaginary components are used to illustrate the evolution of the bright- and dark-soliton solutions for selected parameter values. These graphical representations clarify how fractional temporal scaling modifies the pulse dynamics while preserving the characteristic localized wave profiles. The graphical results illustrate the morphology and fractional-order-dependent trajectories of the exact solutions; they do not constitute a spectral or dynamical stability analysis. Establishing stability would require an independent linearization, eigenvalue analysis, or direct perturbed propagation study.

While auxiliary-based solutions are frequently derived in isolation, a key physical contribution of our analysis is demonstrating how the conformable fractional parameter $\eta$ modulates memory effects in media with cubic-quartic dispersion and power-law nonlinearities. As shown in the subsequent subsections, varying $\eta$ does not merely rescale time statically; it actively reshapes the propagation trajectories and phase structures of both bright and dark solitons, offering valuable control parameters for pulse routing and optical delay applications.

Although the subsequent graphical illustrations focus primarily on the intensity profiles, phase structures, and fractional trajectories of bright and dark solitons, the underlying existence criteria, such as the parameter constraints linking $\gamma$, $\Theta$, and $\Pi$, underscore the active role of gain-loss and dissipative mechanisms. The detuning term $\gamma$ and higher-order perturbative coefficients ensure that the energy exchange between the optical pulse and the surrounding dispersive-dissipative medium remains balanced, maintaining the robust propagation of localized structures over extended distances.

***5.1. Bright-soliton dynamics***

The bright-soliton solution presented in Eq. (31) describes a localized optical wave packet propagating in a nonlinear dispersive medium governed by the fractional complex Ginzburg-Landau equation. For the graphical analysis, the parameters are selected as $\Pi = 0.50, \delta = -4.08, \nu = 5.08, c = 1, \kappa = 0.5, a = -2, b = -1, \gamma = 1, \omega = 1, \alpha = -1, \sigma = 1, n = 2,$ and $\zeta_0 = 1$, whereas the fractional order is varied as $\eta = 0.25, 0.50,$ and $0.75$. The corresponding propagation dynamics are illustrated in Figs. 1-3.

Fig. 1 presents the three-dimensional surfaces, two-dimensional profiles, and contour maps of the absolute, real, and imaginary components of the bright-soliton solution for the fractional order ($\eta = 0.25$). The absolute component exhibits a localized bell-shaped pulse whose maximum amplitude remains nearly constant while its peak shifts with time. The real and imaginary components reveal oscillatory carrier waves confined within the localized sech-shaped envelope. At this relatively low fractional order, the pulse trajectory shows strong nonlinear temporal dependence, indicating pronounced memory effects in the optical medium. This propagation behavior is potentially useful for tunable optical delay lines, slow-light systems, temporal pulse shaping, and information transmission using localized optical pulses.

Fig. 2 illustrates the three-dimensional, two-dimensional, and contour representations of the absolute, real, and imaginary components of the bright-soliton solution for ($\eta$=0.5). The absolute-value plots confirm that the localized pulse preserves its amplitude and spatial width during propagation, whereas the real and imaginary components show phase-modulated oscillations concentrated around the moving pulse center. Compared with the ($\eta$=0.25) case, the pulse follows a modified trajectory because of the different fractional temporal scaling. The combination of stable localization and controllable motion makes this solution relevant to optical-fiber communication, all-optical switching, optical pulse routing, and signal-processing devices requiring robust transmission with limited pulse distortion.

Fig. 3 shows the absolute, real, and imaginary components of the bright-soliton solution for fractional order ($\eta$=0.75) as three-dimensional surfaces, two-dimensional profiles, and contour maps. The localized sech-shaped envelope remains well preserved as it propagates, demonstrating a stable balance between nonlinear and dispersive effects. The real and imaginary components exhibit regular carrier oscillations modulated by the localized envelope, while the contour plots clearly reveal the fractional-order-dependent pulse trajectory. At this higher fractional order, the temporal evolution approaches a more conventional propagation regime, making the resulting bright soliton attractive for high-speed optical transmission, ultrashort-pulse generation, wavelength-division systems, optical sensing, and nonlinear photonic devices.

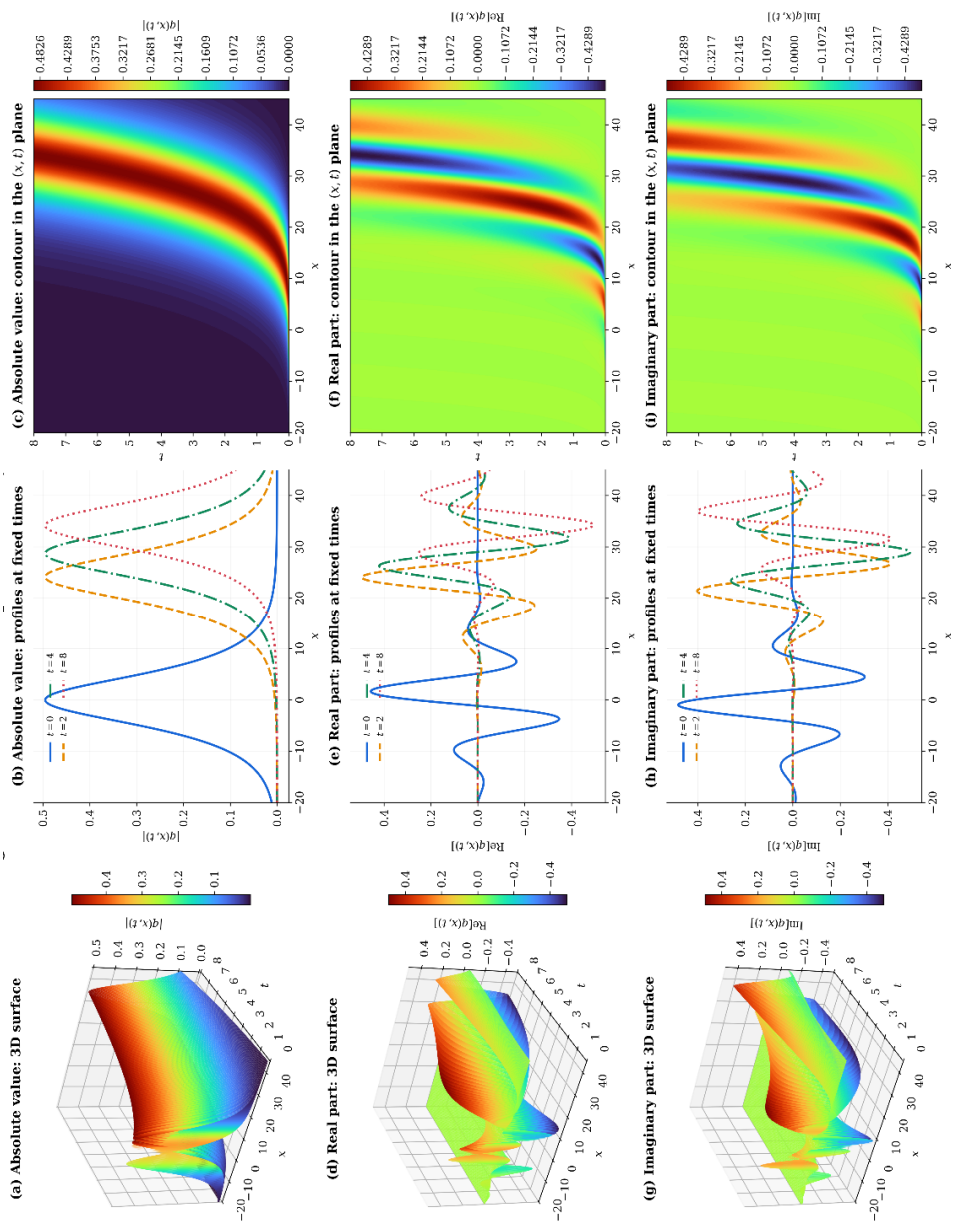



**Fig. 1.** Dark-soliton solution given by Eq. (31) for n=2 and η=0.25.: (a) three-dimensional surface of |q(x,t)|; (b) two-dimensional profiles of |q(x,t)| at (t=0,2,4,8); (c) contour plot of |q(x,t)| in the (x,t)–plane; (d) three-dimensional surface of Re:|q(x,t)|; (e) two-dimensional profiles of Re:|q(x,t)| at (t=0,2,4,8); (f) contour plot of Re:|q(x,t)| in the (x,t)–plane; (g) three-dimensional surface of Im:|q(x,t)|; (h) two-dimensional profiles of Im:|q(x,t)| at (t=0,2,4,8); and (i) contour plot of Im:|q(x,t)| in the (x,t)–plane. The plots are shown over 0≤t≤8 and −20≤t≤45.

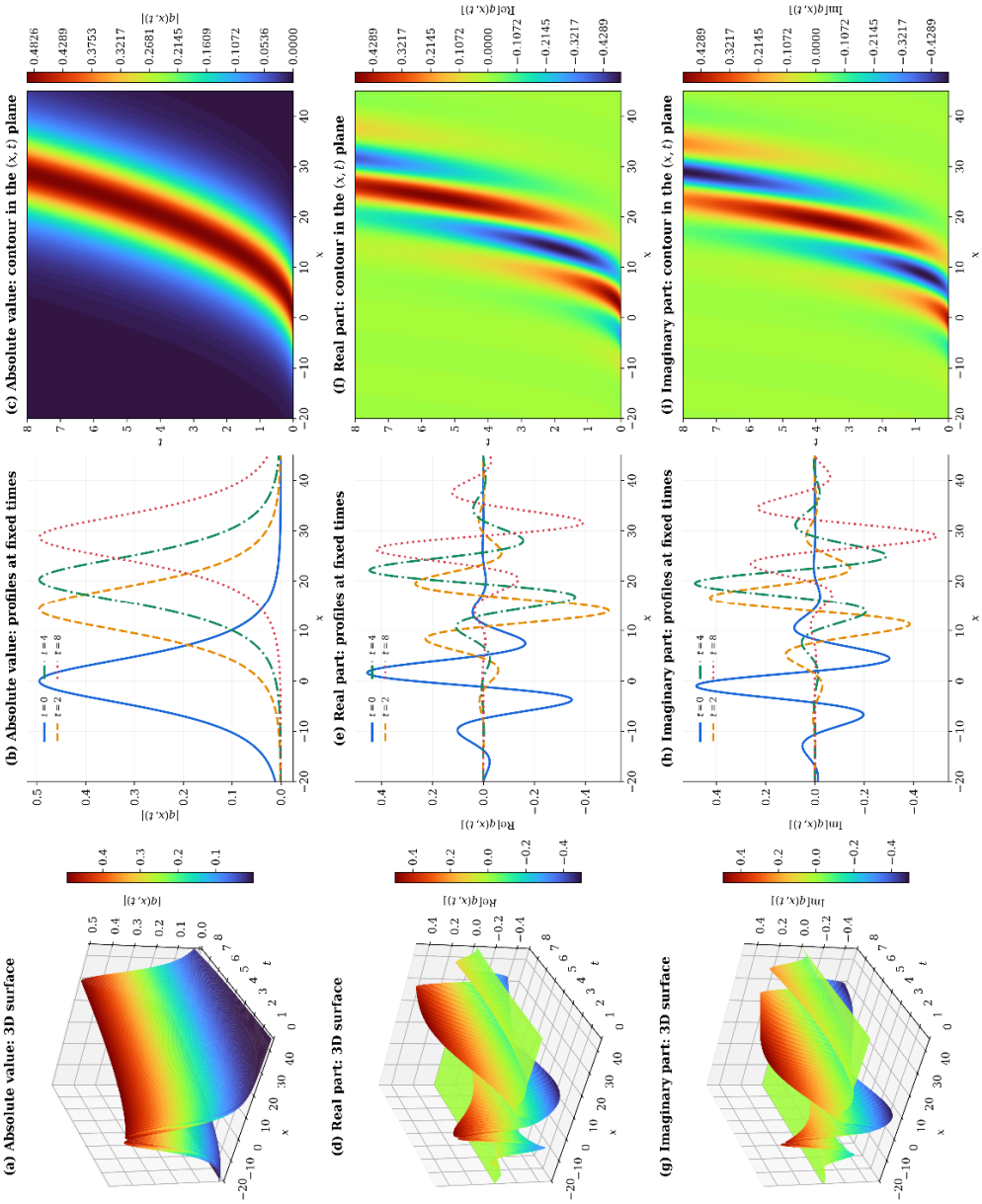



**Fig. 2.** Dark-soliton solution given by Eq. (31) for n=2 and η=0.5.: (a) three-dimensional surface of |q(x,t)|; (b) two-dimensional profiles of |q(x,t)| at (t=0,2,4,8); (c) contour plot of |q(x,t)| in the (x,t)–plane; (d) three-dimensional surface of Re:|q(x,t)|; (e) two-dimensional profiles of Re:|q(x,t)| at (t=0,2,4,8); (f) contour plot of Re:|q(x,t)| in the (x,t)–plane; (g) three-dimensional surface of Im:|q(x,t)|; (h) two-dimensional profiles of Im:|q(x,t)| at (t=0,2,4,8); and (i) contour plot of Im:|q(x,t)| in the (x,t)–plane. The plots are shown over 0≤t≤8 and −20≤t≤45.

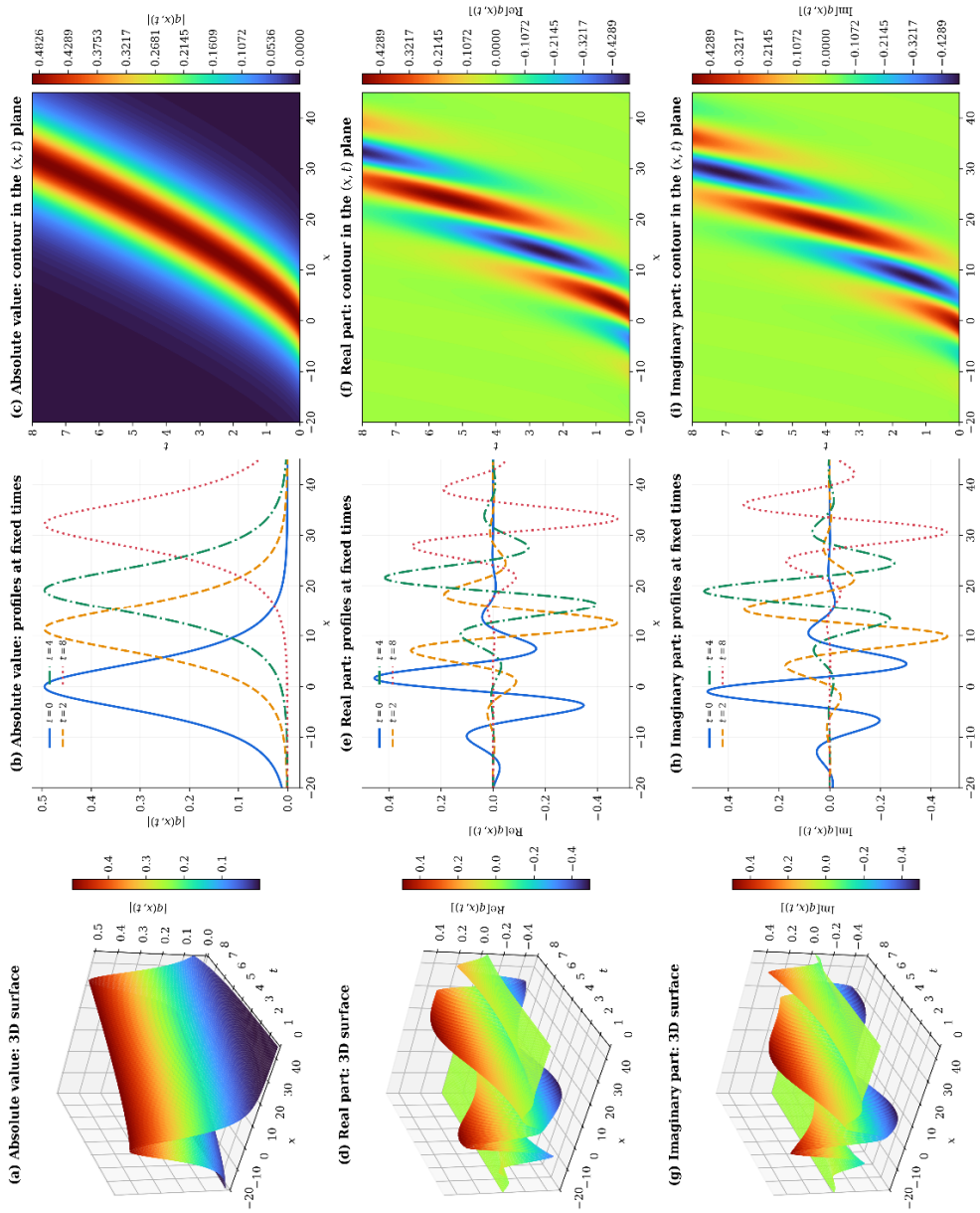



**Fig. 3.** Dark-soliton solution given by Eq. (31) for n=2 and η=0.75.: (a) three-dimensional surface of |q(x,t)|; (b) two-dimensional profiles of |q(x,t)| at (t=0,2,4,8); (c) contour plot of |q(x,t)| in the (x,t)–plane; (d) three-dimensional surface of Re:|q(x,t)|; (e) two-dimensional profiles of Re:|q(x,t)| at (t=0,2,4,8); (f) contour plot of Re:|q(x,t)| in the (x,t)–plane; (g) three-dimensional surface of Im:|q(x,t)|; (h) two-dimensional profiles of Im:|q(x,t)| at (t=0,2,4,8); and (i) contour plot of Im:|q(x,t)| in the (x,t)–plane. The plots are shown over 0≤t≤8 and –20≤t≤45.

### *5.2. Dark-soliton dynamics*

The dark-soliton solution presented in Eq. (35) describes a localized optical wave packet propagating in a nonlinear dispersive medium governed by the fractional complex Ginzburg-Landau equation. For the graphical analysis, the parameters are selected as $\Pi = 0.50, \delta = -4.08, \nu = 5.08, c = -1, \kappa = 0.5, b = 1, \gamma = 1, \omega = 1, \alpha = -1, \sigma = 1, n = 2,$ and $\zeta_0 = 1$, whereas the fractional order is varied as $\eta = 0.25, 0.50$, and $0.75$. The corresponding propagation dynamics are illustrated in Figs. 4-6.

Fig. 4 presents the three-dimensional surface, two-dimensional profiles, and contour maps of the absolute, real, and imaginary components of the dark-soliton solution for the fractional order ($\eta$=0.25). The absolute component shows a localized intensity depression propagating over a continuous-wave background, the defining feature of a dark optical soliton. The real and imaginary components show oscillatory wave structures modulated by the moving dark envelope. At this relatively low fractional order, the trajectory exhibits strong nonlinear temporal dependence, reflecting the stronger influence of conformable fractional temporal scaling on the soliton propagation trajectory. This behavior can be useful in optical pulse shaping, tunable delay systems, and information encoding based on propagating intensity notches.

Fig. 5 depicts the three-dimensional, two-dimensional, and contour representations of the absolute, real, and imaginary components of the dark-soliton solution for ($\eta$=0.5). The absolute-value plots clearly demonstrate the evolution of the localized intensity dip, whereas the real and imaginary plots describe the corresponding oscillatory phase dynamics. Compared with ($\eta$=0.25), the soliton follows a modified propagation trajectory because the fractional temporal evolution changes. This balance between localization and propagation makes the solution relevant to optical-fiber communication, all-optical switching, and signal-processing systems in which controlled dark pulses can serve as robust information carriers.

Fig. 6 illustrates the absolute, real, and imaginary components of the dark-soliton solution for the fractional order ($\eta$=0.75) using three-dimensional surfaces, two-dimensional profiles, and contour maps. The localized minimum in the absolute component remains clearly preserved during propagation, confirming the stability of the dark-soliton structure within the considered domain. Meanwhile, the real and imaginary components exhibit periodic oscillations governed by the carrier phase and modulated by the dark envelope. The higher fractional order produces a distinct temporal trajectory and indicates a transition toward more conventional propagation behavior. These stable, controllable intensity dips have potential applications in high-speed optical transmission, all-optical logic, optical sensing, and manipulating nonlinear waves in dispersive photonic media.

### *5.3. Physical admissibility of solution families*

While the auxiliary expansion method yields a broad spectrum of formal mathematical solutions, distinguishing between physical realizability and mathematical abstraction is essential. The bright and dark soliton solutions maintain finite energy and continuous profiles, rendering them directly relevant to stable optical communications and switching. Conversely, the singular solitons possess singularities that preclude direct physical implementation in standard transmission lines; however, they provide crucial mathematical insights into limiting field localization and wave-breaking regimes. Furthermore, the Jacobi and

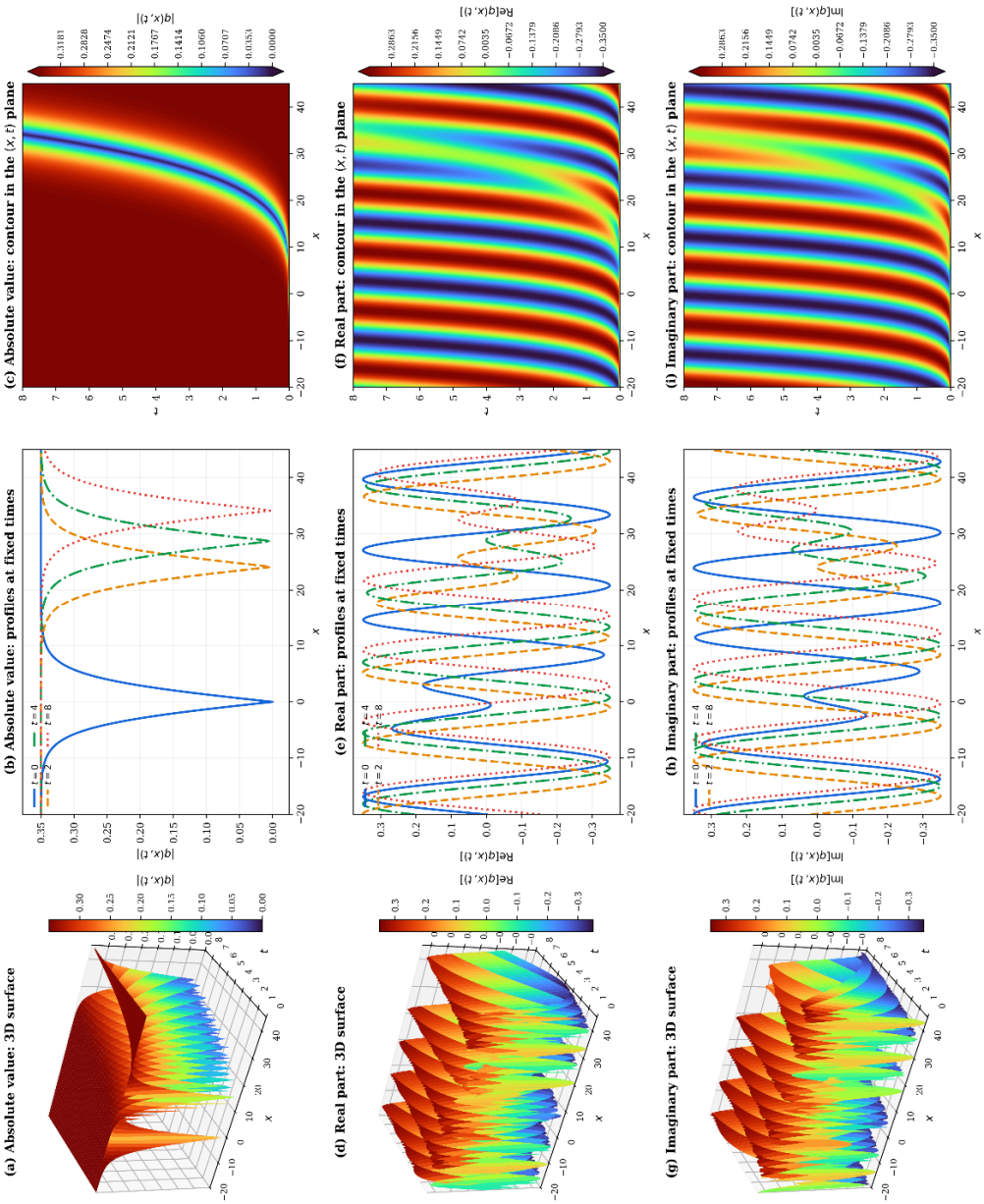



**Fig. 4.** Dark-soliton solution given by Eq. (35) for n=2 and η=0.25.:
(a) three-dimensional surface of |q(x,t)|;
(b) two-dimensional profiles of |q(x,t)| at (t=0,2,4,8);
(c) contour plot of |q(x,t)| in the (x,t)–plane;
(d) three-dimensional surface of Re:|q(x,t)|;
(e) two-dimensional profiles of Re:|q(x,t)| at (t=0,2,4,8);
(f) contour plot of Re:|q(x,t)| in the (x,t)–plane;
(g) three-dimensional surface of Im:|q(x,t)|;
(h) two-dimensional profiles of Im:|q(x,t)| at (t=0,2,4,8); and
(i) contour plot of Im:|q(x,t)| in the (x,t)–plane. The plots are shown over 0≤t≤8 and −20≤t≤45.

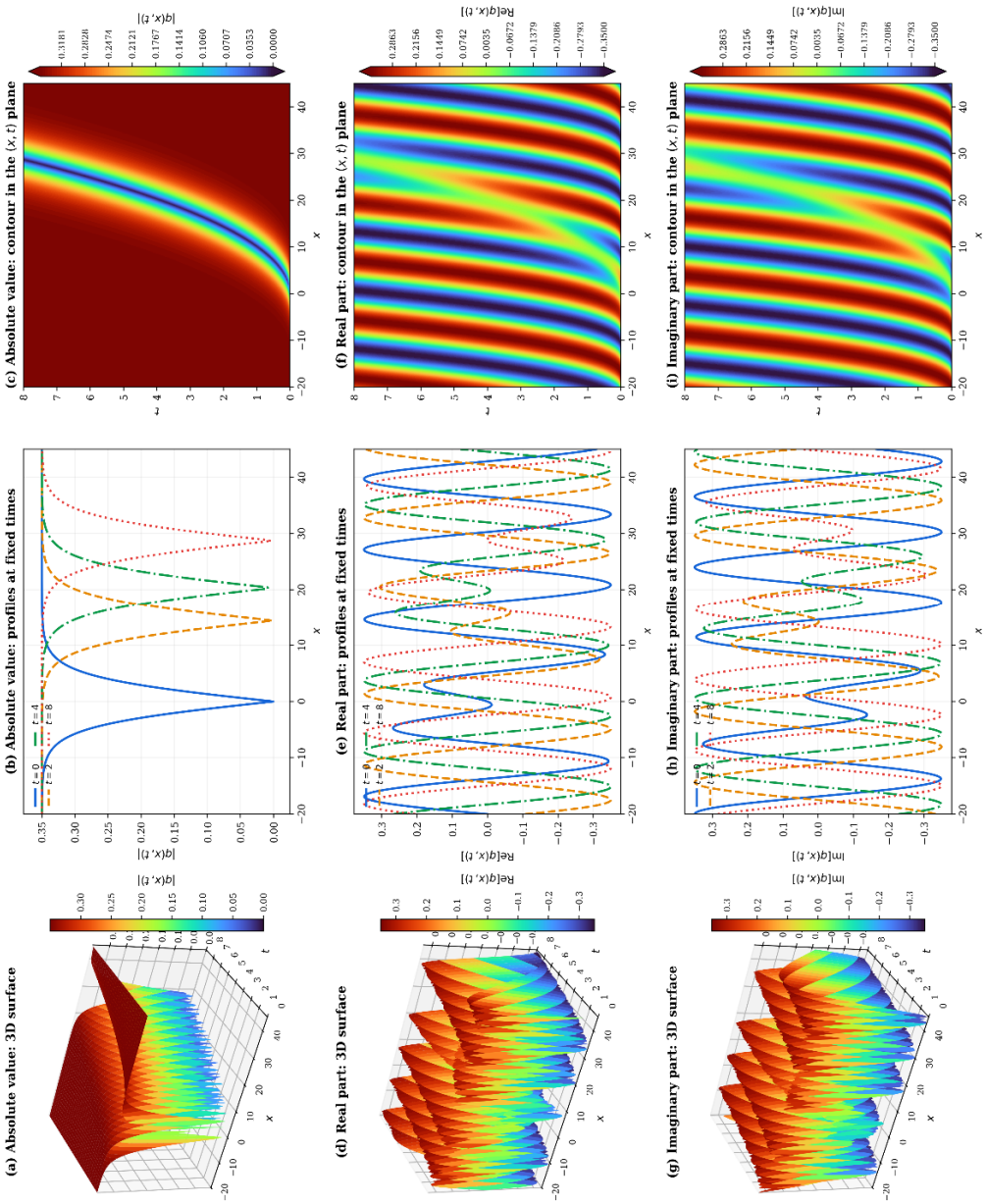



**Fig. 5.** Dark-soliton solution given by Eq. (35) for n=2 and η=0.5.:
(a) three-dimensional surface of |q(x,t)|;
(b) two-dimensional profiles of |q(x,t)| at (t=0,2,4,8);
(c) contour plot of |q(x,t)| in the (x,t)−plane;
(d) three-dimensional surface of Re:|q(x,t)|;
(e) two-dimensional profiles of Re:|q(x,t)| at (t=0,2,4,8);
(f) contour plot of Re:|q(x,t)| in the (x,t)−plane;
(g) three-dimensional surface of Im:|q(x,t)|;
(h) two-dimensional profiles of Im:|q(x,t)| at (t=0,2,4,8); and
(i) contour plot of Im:|q(x,t)| in the (x,t)−plane. The plots are shown over 0≤t≤8 and −20≤t≤45.

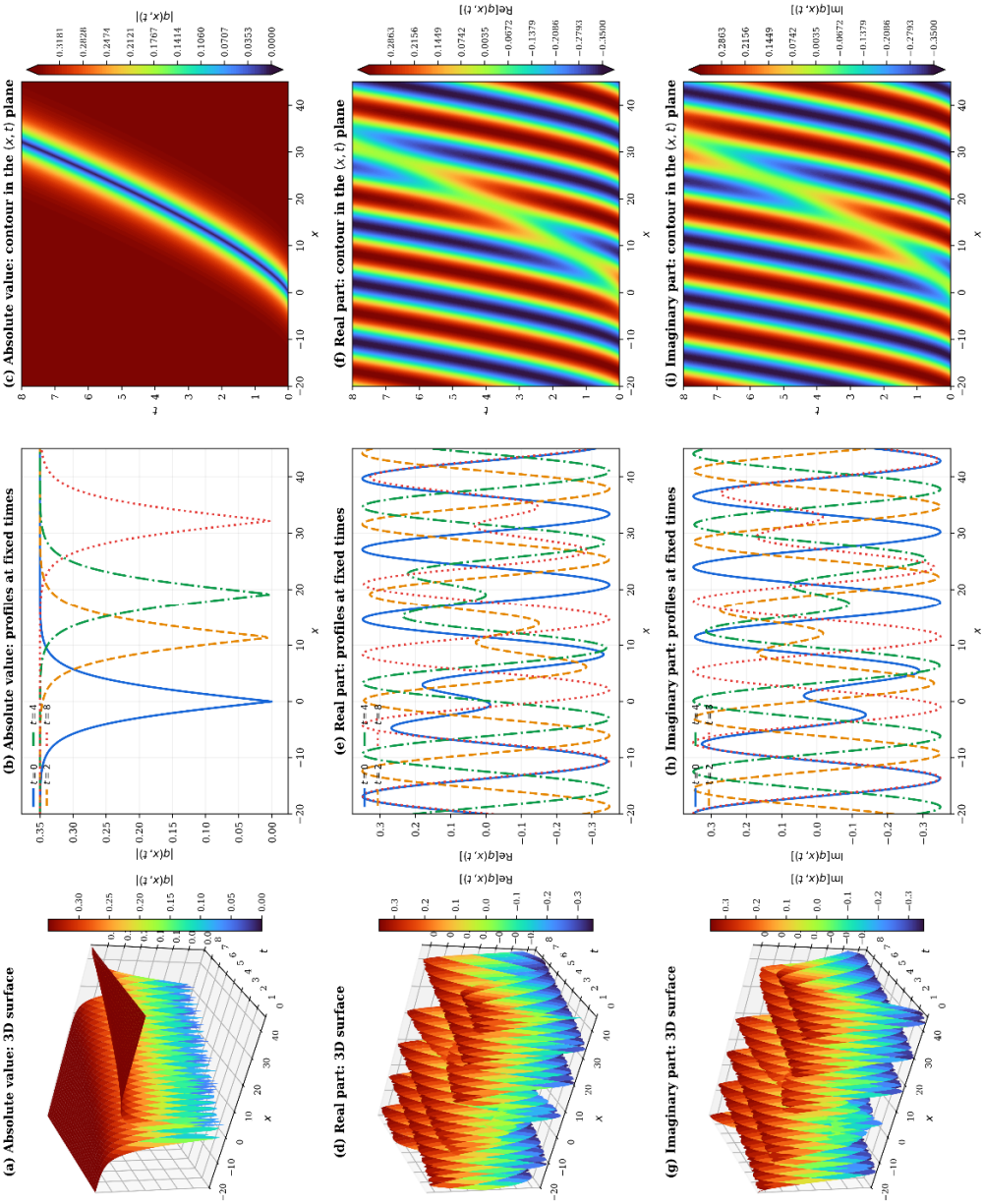



**Fig. 6.** Dark-soliton solution given by Eq. (35) for n=2 and η=0.75.: (a) three-dimensional surface of |q(x,t)|; (b) two-dimensional profiles of |q(x,t)| at (t=0,2,4,8); (c) contour plot of |q(x,t)| in the (x,t)–plane; (d) three-dimensional surface of Re:|q(x,t)|; (e) two-dimensional profiles of Re:|q(x,t)| at (t=0,2,4,8); (f) contour plot of Re:|q(x,t)| in the (x,t)–plane; (g) three-dimensional surface of Im:|q(x,t)|; (h) two-dimensional profiles of Im:|q(x,t)| at (t=0,2,4,8); and (i) contour plot of Im:|q(x,t)| in the (x,t)–plane. The plots are shown over 0≤t≤8 and −20≤t≤45.

Weierstrass elliptic function solutions represent physically viable periodic wave trains and pulse lattices within specific modulus bounds ( $0 \le m \le 1$ ), making them useful for analyzing periodic modulation and nonlinear multi-mode interactions in optical cavities.

## 6. Conclusion

In this work, cubic-quartic optical solitons were investigated for a conformable time-fractional complex Ginzburg-Landau equation with power-law self-phase modulation. The governing model incorporated third- and fourth-order dispersion, intermodal dispersion, self-steepening, and higher-order nonlinear dispersive perturbations. By introducing a conformable fractional traveling-wave transformation and separating the resulting equation into its real and imaginary components, the model was reduced to a fourth-order nonlinear ordinary differential equation. This reduction also established the compatibility and integrability conditions needed to construct exact traveling-wave solutions.

The principal novelty of the present study lies in the unified analytical treatment of cubic-quartic dispersion and general power-law self-phase modulation within a conformable time-fractional complex Ginzburg-Landau framework. In contrast to previous investigations primarily addressing lower-order dispersive models, conventional integer-order formulations, or particular nonlinear responses, the present work simultaneously incorporates higher-order dispersion, fractional temporal evolution, and power-law nonlinearity into the analytical solution procedure. Furthermore, we established explicit compatibility and parameter-existence conditions for the resulting solution families, providing a systematic characterization of their mathematical admissibility.

Using the extended auxiliary equation method, we constructed several families of exact solutions, including bright, dark, and singular solitons, along with periodic solutions expressed in terms of Jacobi and Weierstrass elliptic functions. Another important contribution is the graphical examination of how different conformable fractional orders influence the effective temporal scaling, phase evolution, and propagation trajectories of representative bright and dark solitons. The results demonstrate that varying the fractional order modifies the propagation trajectories while preserving the characteristic localized bright envelopes and dark intensity depressions within the considered parameter ranges.

Overall, the present findings extend the analytical description of nonlinear optical waves in higher-order dispersive systems with power-law responses and conformable fractional temporal evolution. The derived solutions provide useful analytical benchmarks for future numerical investigations of nonlinear pulse propagation. Further research should focus on spectral and dynamical stability, sensitivity to parameter perturbations and noise, and the applicability of the obtained solution families to experimentally realizable optical-fiber and photonic systems.

**Funding and acknowledgement.** The authors extend their appreciation to King Saud University, Saudi Arabia, for funding this work through the Ongoing Research Funding Program (ORF-2026-704), King Saud University, Riyadh, Saudi Arabia. This work for the last author was supported by Grambling State University for the Endowed Chair of Mathematics. This support is gratefully acknowledged. No additional grants have been received to conduct or direct this particular study.

**Data Availability Statement.** The original contributions presented in this study are included in the article. Further inquiries can be directed to the corresponding author.

**Conflicts of Interest.** The authors declare no conflicts of interest.

**Author Contributions.** Mohamed Sharaf: methodology, formal analysis, and writing – original draft. Mohamed E. M. Alngar: methodology, software, visualization, investigation, data curation, writing–review & editing, analytical calculations, and validation. Reham M. A. Shohib: software, visualization, and validation. Houria Triki: conceptualization, methodology, writing – review and editing. Syed Asif Ali Shah: formal analysis and writing – review and editing. Anjan Biswas: conceptualization, supervision, validation, writing – review and editing. All authors have read and agreed to the published version of the manuscript.

## References


1. Iqbal, M., Faridi, W. A., Algethamie, R., Aljohani, A., El-Meligy, M., Mohammad, N., & Alnowibet, K. A. (2025). Propagation of optical solitons and dispersive solitary wave structure in complex media to the nonlinear integrable system via computational technique. *Scientific Reports*, *15*(1), Article 38317.
2. Mustafa, M. A., & Murad, M. A. S. (2025). Optical solutions of the nonlinear conformable Schrödinger equation in weakly non-local media using two distinct analytic methods. *Nonlinear Dynamics*, *113*(15), 20105–20119.
3. Bibi, I., Muhammad, S., Shakeel, M., & Ceesay, B. (2025). Optical soliton structure solutions, sensitivity, and modulation stability analysis in the chiral nonlinear Schrödinger equation with Bohm potential. Advances in *Mathematical Physics*, *2025*(1), Article 9185387.
4. Borah, B., Sarmah, D. R., & Phukan, D. (2025). Parametric analysis of pulsating soliton dynamics in fiber laser using the complex Ginzburg-Landau framework. *Journal of Optics*.
5. Hasegawa, A. (2022). Optical soliton: Review of its discovery and applications in ultra-high-speed communications. *Frontiers in Physics*, *10*, Article 1044845.
6. Arnous, A. H., Murad, M. A. S., Yildirim, Y., & Biswas, A. (2026). Quiescent vector optical solitons with nonlinear dispersion. *Ukrainian Journal of Physical Optics*, *27*(4), 04054–04076.
7. Kaur, L., Arnous, A. H., Murad, M. A. S., & Biswas, A. (2026). Dispersive optical soliton perturbation with Schrödinger-Hirota equation by Lie symmetry. *Ukrainian Journal of Physical Optics*, *27*(3), 03238–03258.
8. Adem, A. R., Arnous, A. H., Calucag, L. S., & Biswas, A. (2026). Implicit quiescent soliton perturbation in optical metamaterials with nonlinear chromatic dispersion and Kudryashov's quintuple form of self-phase modulation by Lie symmetry. *Ukrainian Journal of Physical Optics*, *27*(3), 03009–03019.
9. Yıldırım, Y., Biswas, A., Khan, S., Mahmood, M. F., & Alshehri, H. M. (2022). Highly dispersive optical soliton perturbation with Kudryashov's sextic-power law of nonlinear refractive index. *Ukrainian Journal of Physical Optics*, *23*(1), 24–29.
10. Zhou, Q., Zhong, Y., Mirzazadeh, M., Bhrawy, A. H., Zerrad, E., & Biswas, A. (2016). Thirring combo-solitons with cubic nonlinearity and spatio-temporal dispersion. *Waves in Random and Complex Media*, *26*(2), 204–210.
11. Metwally, A. S. M., Alngar, M. E. M., Shohib, R. M. A., Shirsath, S. E., & Biswas, A. (2026). Stochastic (3+1)-dimensional spatio-temporal solitons in a generalized effective fiber Bragg-grating envelope model. *Ukrainian Journal of Physical Optics*, *27*(4), 04102–04127.
12. Samina, S., Munawar, M., Ansari, A. R., Jhangeer, A., & Wali, S. (2025). Nonlinear optical dynamics and complex wave structures in nonlinear dispersive media. *Scientific Reports*, *15*(1), Article 15562.
13. Ahmad, J., Mustafa, Z., & Habib, J. (2024). Analyzing dispersive optical solitons in nonlinear models using an analytical technique and its applications. *Optical and Quantum Electronics*, *56*(1), Article 77.
14. Gassem, F., Osman, O., Alqarni, F., Aldwoah, K., Birkea, F. M. O., & Hleili, M. (2025). A novel approach to construct optical solitons solutions of complex Ginzburg–Landau equation with five distinct forms of nonlinearities. *Alexandria Engineering Journal*, *113*, 551–564.
15. Li, X., Cui, X., & Zhang, S. (2025). Analysis of a Crank–Nicolson fast element-free Galerkin method for the nonlinear complex Ginzburg–Landau equation. *Journal of Computational and Applied Mathematics*, *457*, Article 116323.
16. Rateb, A. E., Ahmed, H. M., Darwish, A., Ammar, M., & Rabie, W. B. (2026). Analytical wave families and stability dynamics in a modified complex Ginzburg–Landau model via the modified extended direct algebraic method. *Scientific Reports*, *16*(1), Article 7485.
17. Chou, D., Amer, A., Rehman, H. U., & Li, M.-L. (2025). Unravelling quiescent optical solitons: An exploration of the complex Ginzburg–Landau equation with nonlinear chromatic dispersion and self-phase modulation. *Nonlinear Engineering*, *14*(1), Article 20240043.
18. Wang, K.-J., Zhu, H.-W., Li, S., Shi, F., Li, G., & Liu, X.-L. (2025). Bifurcation analysis, chaotic behaviors, variational principle, Hamiltonian and diverse optical solitons of the fractional complex Ginzburg–Landau model. *International Journal of Theoretical Physics*, *64*(5), Article 134.

19. Kumar, S., Sharma, S. K., Karwasra, R., Malik, S., Nofal, T. A., & Arnous, A. H. (2025). Soliton structures, bifurcation patterns, and chaos in a nonlinear transmission line governed by the modified complex Ginzburg–Landau equation. *Chaos, Solitons & Fractals*, *200*(Part 2), Article 117068.
20. Li, X., & Kai, Y. (2025). A complete study of the Wick-type stochastic complex Ginzburg–Landau equation. *Modern Physics Letters B*, *39*(29), Article 2550176.
21. Biswas, A., Yıldırım, Y., Ekici, M., Guggilla, P., Khan, S., González-Gaxiola, O., & Belic, M. R. (2021). Cubic-quartic optical soliton pertubation with complex Ginzburg-Landau equation. *Journal of Applied Science and Engineering*, *24*(6), 937–1004.
22. Arshed, S. (2018). Soliton solutions of fractional complex Ginzburg-Landau equation with Kerr law and non-Kerr law media. *Optik*, *160*, 322–332.
23. Akbulut, A. (2023). Obtaining the soliton type solutions of the conformable time-fractional complex Ginzburg-Landau equation with Kerr law nonlinearity by using two kinds of Kudryashov methods. *Journal of Mathematics*, *2023*, Article 4741219.
24. Al-Ghafri, K. S. (2020). Soliton behaviours for the conformable space-time fractional complex Ginzburg-Landau equation in optical fibers. *Symmetry*, *12*(2), Article 219.
25. Shi, L.-F., Chen, C.-S., & Zhou, X.-C. (2011). The extended auxiliary equation method for the KdV equation with variable coefficients. *Chinese Physics B*, *20*(10), Article 100507.
26. Xu, G.-Q. (2014). Extended auxiliary equation method and its applications to three generalized NLS equations. *Abstract and Applied Analysis*, *2014*, Article 541370.
27. Zayed, E. M. E., & Alurrfi, K. A. E. (2016). Extended auxiliary equation method and its applications for finding the exact solutions for a class of nonlinear Schrödinger-type equations. *Applied Mathematics and Computation*, *289*, 111–131.
28. Khalil, R., Al Horani, M., Yousef, A., & Sababheh, M. (2014). A new definition of fractional derivative. *Journal of Computational and Applied Mathematics*, *264*, 65–70.

Sharaf, M., Alngar, M.E.M., Shohib, R.M.A., Triki, H., Shah, S.A.A., & Biswas, A. (2027). Cubic-Quartic Optical Solitons with Complex Ginzburg-Landau Equation Having Power-Law of Self-Phase Modulation and Fractional Temporal Evolution. *Ukrainian Journal of Physical Optics*, *28*(1), 01089 – 01111.
doi: 10.3116/16091833/Ukr.J.Phys.Opt.2027.01089

***Анотація.*** *У цьому дослідженні розглядаються оптичні солітони, що описуються комплексним рівнянням Гінзбурга—Ландау з конформною дробовою похідною за часом і степеневою самофазовою модуляцією. Модель враховує дисперсію третього та четвертого порядків, міжмодову дисперсію, ефект самокрутизни, а також нелінійні дисперсійні збурення. Застосування підстановки у вигляді біжучої хвилі дозволяє звести вихідне рівняння до нелінійного звичайного диференціального рівняння четвертого порядку, а прирівнювання його дійсної та уявної частин дає змогу отримати умови сумісності та інтегровності. Для знаходження точних розв'язків – світлих, темних і сингулярних солітонів, а також періодичних розв'язків, виражених через еліптичні функції Якобі та Вейєрштрасса, використано розширений метод допоміжних рівнянь. Також наведено явні умови існування цих розв'язків. Графічні ілюстрації демонструють вплив конформного дробового порядку на ефективний часовий масштаб, фазову структуру та динаміку поширення світлих і темних солітонів. Отримані розв'язки розширюють аналітичний опис нелінійних хвиль в оптичних системах із дисперсією вищих порядків і можуть слугувати еталонними розв'язками для подальших чисельних досліджень та аналізу стійкості.*

***Ключові слова:*** *оптичні солітони, рівняння Гінзбурга—Ландау з дробовою похідною, степенева нелінійність, дисперсія третього та четвертого порядків, розширений метод допоміжних рівнянь, розв'язки еліптичних функцій.*